BIOCHEMISTRY
including biophysical chemistry & molecular biology

Article

pubs.acs.org/biochemistry

Mechanism of Drug–Drug Interactions Mediated by Human Cytochrome P450 CYP3A4 Monomer

Ilia G. Denisov,[†] Yelena V. Grinkova,[†] Javier L. Baylon,[‡,§] Emad Tajkhorshid,[†,‡,§] and Stephen G. Sligar*[,†,‡]

[†]Department of Biochemistry, [‡]Center for Biophysics and Computational Biology, and [§]Beckman Institute for Advanced Science and Technology, University of Illinois at Urbana-Champaign, Urbana, Illinois 61801, United States

ABSTRACT: Using Nanodiscs, we quantitate the heterotropic interaction between two different drugs mediated by monomeric CYP3A4 incorporated into a nativelike membrane environment. The mechanism of this interaction is deciphered by global analysis of multiple-turnover experiments performed under identical conditions using the pure substrates progesterone (PGS) and carbamazepine (CBZ) and their mixtures. Activation of CBZ epoxidation and simultaneous inhibition of PGS hydroxylation are measured and quantitated through differences in their respective affinities for both a remote allosteric site and the productive catalytic site near the heme iron. Preferred binding of PGS at the allosteric site and a stronger preference for CBZ binding at the productive site give rise to a nontrivial drug–drug interaction. Molecular dynamics simulations indicate functionally important conformational changes caused by PGS binding at the allosteric site and by two CBZ molecules positioned inside the substrate binding pocket. Structural changes involving Phe-213, Phe-219, and Phe-241 are thought to be responsible for the observed synergetic effects and positive allosteric interactions between these two substrates. Such a mechanism is likely of general relevance to the mutual heterotropic effects caused by biologically active compounds that exhibit different patterns of interaction with the distinct allosteric and productive sites of CYP3A4, as well as other xenobiotic metabolizing cytochromes P450 that are also involved in drug–drug interactions. Importantly, this work demonstrates that a monomeric CYP3A4 can display the full spectrum of activation and cooperative effects that are observed in hepatic membranes.

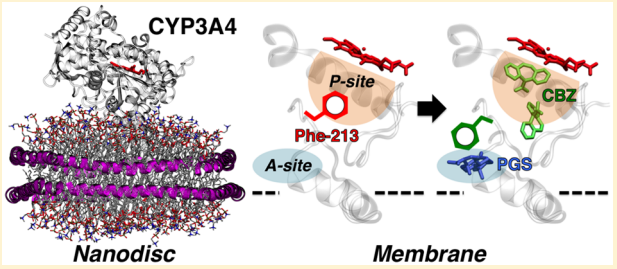

Cytochromes P450 make up a key class of enzymes involved in the metabolism of xenobiotics, with the CYP3A4 isoform in human liver being responsible for many critical biotransformations. Given their involvement in the metabolism of numerous drugs, these enzymes constitute a major site of drug–drug interactions. CYP3A4 can bind multiple copies of many compounds, and the enzyme often exhibits cooperativity with multiple substrates. Very often, these interactions are detected as inhibition of CYP3A4-mediated metabolism of test substrates by the presence of an effector or another compound,[1] which can result in a dangerously high concentration of an administered therapeutic. Some compounds can accelerate CYP3A4-mediated metabolism *in vitro*, e.g., α-naphthoflavone (ANF),[2] quinidine,[3] steroids,[4] and a number of potential drug candidate molecules.[5] This metabolic interaction between two different compounds is termed "heterotropic" and, like the homotropic case, is manifested through the simultaneous binding of multiple molecules to the enzyme. Despite the importance of CYP3A4 to human pharmacology, the detailed mechanisms of such heterotropic effects are not completely understood. Given different systems and protocols employed by various research groups, it has been difficult to directly compare the reported results, leading to confusion and conflicting claims. For instance, ANF was stated to be both an inhibitor[6,7] and an activator of CYP3A4.[8−10] Further complications arise when one considers the possibility of oligomeric complexes of multiple P450s.[10]

The anticonvulsant drug carbamazepine (CBZ) has been reported to increase the rate of clearance of warfarin,[11] and this positive heterotropic effect has been attributed to induction of CYP3A4.[12] Direct interaction of CBZ with the sedative drug midazolam inside the substrate binding pocket has been suggested to be the molecular basis underlying the observed changes in stereospecificity of midazolam hydroxylation.[13] The accelerated metabolism of steroids (including oral contraceptives) during CBZ administration has also been attributed to the induction of CYP3A4.[14−16] On the other hand, CBZ has been reported to act as an inhibitor of hydroxylation of both steroids and midazolam *in vitro*,[13,17] while 10,11-epoxidation of CBZ by CYP3A4 is activated in the presence of various endogenous steroids[4,17,18] as well as other effectors, e.g., ANF, artemisinin, and quinidine.[19]

To understand the mechanism of heterotropic cooperativity in monomeric CYP3A4, we initiated a series of experimental studies using a pair of substrates with substantially different physical properties, namely, the clinically relevant steroid

Received: January 27, 2015
Revised: March 13, 2015
Published: March 17, 2015

DOI: 10.1021/acs.biochem.5b00079
Biochemistry 2015, 54, 2227−2239

progesterone (PGS) and the anti-epileptic drug CBZ. Both drugs are known CYP3A4 substrates, and their mutual metabolic effects have been reported in several previous studies, although no mechanistic interpretation was provided for the observed heterotropic interactions.[17,19] In addition, both drugs can act as allosteric effectors, activating the metabolism of other substrates (PGS and other steroids activate CBZ epoxidation[19]) or changing the regioselectivity of hydroxylation for other substrates catalyzed by CYP3A4.[13] However, their relative affinities with respect to the productive binding site inside the substrate binding pocket near the heme iron (P-site) and to the nonproductive allosteric binding site (A-site) are anticipated to be distinct because of the differences in their molecular shape and solubility. Importantly, heterotropic effects could be most pronounced in the mixture of two substrates with preferential affinities for the productive site (P-type substrate) for one and the allosteric site (A-type substrate) for the other. In such a case, preferential binding of the A-type substrate to the allosteric site is expected to favor binding and metabolism of the P-type substrate inside the binding pocket, if its affinity for the latter is higher.

In addition to the experimental investigations focused on determining the fundamental catalytic properties of CYP3A4 in its multiple substrate-bound states, we also performed a series of molecular dynamics (MD) simulations of the CYP3A4 monomer in a membrane environment, with CBZ and PGS bound to the enzyme. The allosteric site of CYP3A4 located near the membrane interface was probed with PGS and CBZ in independent simulations to study the dynamics of the two substrates at this nonproductive binding site. The dynamics of CBZ near the productive site of CYP3A4 were probed using both one and two copies of this substrate in the active site and provided critical structural insight into the mechanism of heterotropic cooperativity of CYP3A4.

EXPERIMENTAL PROCEDURES

Protein Expression and Purification. Expression and purification of membrane scaffold protein (MSP), cytochrome P450 CYP3A4, and rat P450 reductase, as well as preparation of CYP3A4 in POPC Nanodiscs (ND), were executed following previously described protocols.[20−22] Cytochrome P450 CYP3A4 was expressed from the NF-14 construct in the PCWori+ vector with a C-terminal pentahistidine tag generously provided by F. P. Guengerich (Vanderbilt University, Nashville, TN). Cytochrome P450 reductase (CPR) was expressed using the rat CPR/pOR262 plasmid, a generous gift from T. D. Porter (University of Kentucky, Lexington, KY). Incorporation of CPR into preformed and purified CYP3A4 Nanodiscs was made by direct addition of CPR at a 1:4 CYP3A4:CPR molar ratio, as described previously.[23] All experiments were performed at 37 °C using a POPC Nanodisc system analogous to our previously detailed mechanistic studies[24,25] to allow direct comparison of results. This reconstitution system provides a stable well-characterized and monodisperse preparation of CYP3A4 incorporated into the model lipid bilayer effectively mimicking the native membrane.

UV−Vis Spectroscopy. Substrate titration experiments were performed at 1 μM CYP3A4 in Nanodiscs using a Cary 300 spectrophotometer (Varian, Lake Forest, CA) at 37 °C. For the mixed titration experiments, the mixtures of steroid substrate PGS with CBZ in methanol were prepared and added to the CYP3A4 Nanodisc solution, thereby maintaining the constant substrate ratios. The final concentration of methanol was <1.5%.

NADPH Oxidation and Product Formation. CYP3A4-incorporated Nanodiscs with CPR in a 1:4 molar ratio and substrate were preincubated for 5 min at 37 °C in a 1 mL reaction volume in 100 mM HEPES buffer (pH 7.4), 10 mM $MgCl_2$, and 0.1 mM dithiothreitol. The concentration of CYP3A4 was in the range from 60 to 100 nM. The reaction was initiated with the addition of 200 nmol of NADPH. NADPH consumption was monitored for 5 min and calculated from the absorption changes at 340 nm using an extinction coefficient of 6.22 mM^{-1} cm^{-1}. A short reaction time was used to avoid covalent modification of CYP3A4 by CBZ.[26] At the end of the incubation period, 0.5 mL of the sample was removed from the cuvette, mixed with 2 mL of dichloromethane, and used for product analysis. Cortexolone (2.5 nmol per sample) was added as an internal standard. The samples were thoroughly mixed; after phase separation, the organic layer was isolated and the solvent was removed under a stream of nitrogen. The dried sample was dissolved in 70 μL of methanol, and 40 μL was injected onto an Ace 3 C18 HPLC column (2.1 mm × 150 mm) (MAC-MOD Analytical, Chadds Ford, PA). The mobile phase contained 15% acetonitrile and 15% methanol in water; products of PGS hydroxylation and CBZ epoxidation were separated in a linear gradient of acetonitrile and methanol rising from 15 to 37% each over 35 min at a flow rate of 0.2 mL/min. Calibration and method validation were performed using commercially available metabolites of PGS and CBZ. The chromatograms were processed with Millennium (Waters).

Global Analysis for Deconvoluting Apparent Cooperative Effects in P450. Global analysis of homotropic cooperativity for metabolism of one substrate was performed, as previously described,[24] by simultaneously fitting the experimental data sets to the four-state linear equilibrium binding scheme:

$$E + S \leftrightarrow ES + S \leftrightarrow ES_2 + S \leftrightarrow ES_3$$

where E is the concentration of substrate-free CYP3A4 (designated [**00**] in Scheme 1), S is the concentration of the

Scheme 1. Binding Equilibria for a CYP3A4 Monomer with Three Binding Sites[a]

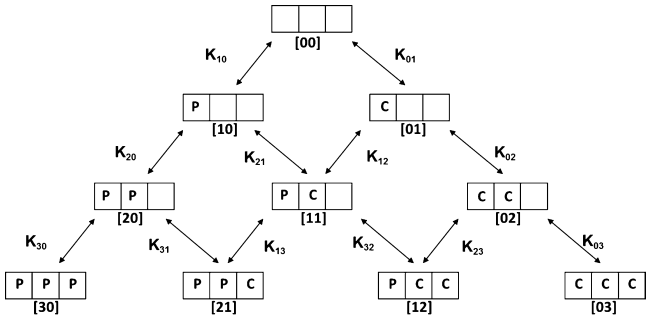

[a]Two types of substrates designated P (PGS) and C (CBZ) can bind to the same or similar binding sites, so that up to three substrate molecules can bind to one CYP3A4 monomer. The fractional populations of all 10 binding intermediates are determined by the 12 equilibrium constants K_{ij}. Three additional equations determined by the microscopic reversibility in the closed cycles ($K_{10}K_{21} = K_{01}K_{12}$, $K_{20}K_{31} = K_{21}K_{13}$, and $K_{12}K_{32} = K_{02}K_{23}$) reduce the number of independent constants from 12 to 9. See the text for a further description.

DOI: 10.1021/acs.biochem.5b00079
Biochemistry 2015, 54, 2227−2239

free substrate, and ES_i terms are the concentrations of the binding intermediates, i.e., complexes of CYP3A4 with i molecules of substrate bound (i = 1, 2, or 3). These binding intermediates are designated [**10**], [**20**], and [**30**] for one substrate and [**01**], [**02**], and [**03**] for another (Scheme 1), with stoichiometric dissociation constants K_{i0} and K_{oi} (i = 1, 2, or 3). Binding of up to three molecules of these substrates to one CYP3A4 monomer was described in previous studies,[27−29] and attempts to fit the data with only two binding sites proved to be unsuccessful.

The fractions of the enzyme−substrate complexes were expressed using the standard binding polynomials[30]

$$Y = \frac{\frac{S}{K_{10}} + \frac{S^2}{K_{10}K_{20}} + \frac{S^3}{K_{10}K_{20}K_{30}}}{1 + \frac{S}{K_{10}} + \frac{S^2}{K_{10}K_{20}} + \frac{S^3}{K_{10}K_{20}K_{30}}}$$

with the functional properties at different substrate concentrations represented as the linear combination of the fractional contributions from binding intermediates. For example, the fraction of the high-spin CYP3A4 in type I titrations, Y_S, is calculated as the weighted sum of the signals from the cytochrome P450 molecules with 0, 1, 2, or 3 substrate molecules bound, having a_0, a_1, a_2, and a_3 fractions of the high-spin state, respectively:

$$Y_S = \frac{a_0 + \frac{a_1 S}{K_{10}} + \frac{a_2 S^2}{K_{10}K_{20}} + \frac{a_3 S^3}{K_{10}K_{20}K_{30}}}{1 + \frac{S}{K_{10}} + \frac{S^2}{K_{10}K_{20}} + \frac{S^3}{K_{10}K_{20}K_{30}}}$$

The set of such equations for the spectral titration, NADPH consumption, and product formation has been used for the simultaneous fitting of the experimental data obtained under the same conditions, using the same set of dissociation constants, which then corresponds to a total of 12 parameters. The fitting program was written in MATLAB using the Nelder−Mead simplex minimization algorithm implemented in the MATLAB subroutine "fminsearch.m".

Heterotropic interactions were analyzed using the system of stoichiometric equilibria shown in Scheme 1. A complete description of 10 states with different combinations of two substrates that can bind at three binding site requires 12 binding constants, although only nine of them are independent variables (Scheme 1 and its footnote). The functional properties of these binding intermediates cannot be individually measured for the pure states with the exception of [**00**] and possibly [**30**] and [**03**], if substrate saturation can be reached. However, the 10-state system can be efficiently separated into three parts by the choice of experimental conditions. The homotropic paths [**00**] → [**10**] → [**20**] → [**30**] and [**00**] → [**01**] → [**02**] → [**03**] can be measured separately with only one substrate, as described above and in our previous publications.[25] Subsequently, the full sets of obtained parameters can be used for the experiments with the mixture of two substrates, if all experiments are performed under identical conditions. In this case, only three equilibrium dissociation constants, K_{11}, K_{12}, and K_{21}, and other functional properties for three mixed intermediates [**11**], [**21**], and [**12**] need to be resolved from the similar set of experiments, with the number of unknown parameters being the same as for the homotropic problem, and can be successfully treated using global analysis.[24,25,31] This was done using the same approach as outlined above for the global analysis of homotropic experiments. Cooperative free energies $\Delta\Delta G$ for the mixed intermediates [**11**], [**21**], and [**12**] were calculated from ratios of corresponding stoichiometric binding constants obtained in fitting: $\Delta\Delta G_{11} = RT \ln(K_{21}/K_{20})$, $\Delta\Delta G_{21} = RT \ln(K_{31}/K_{30})$, and $\Delta\Delta G_{12} = RT \ln(K_{23}/K_{03})$, where RT = 0.617 kcal/mol at 310 K.

COMPUTATIONAL PROCEDURES

CYP3A4 Model and Initial Configurations. A membrane-bound model of the globular domain of CYP3A4 (Protein Data Bank entry 1TQN[32]), including the transmembrane helix formed by residues 1−27, was adopted from the last frame of one of the membrane binding simulations reported previously.[33] The system is composed of CYP3A4 bound to a solvated POPC membrane. This system was then minimized for 1000 steps and equilibrated for 100 ps while restraining the heavy atoms of the protein and the lipids within 3.5 Å of the protein with a force constant k of 1 kcal mol^{-1} Å^{-2}. Following this step, the system was simulated without restraints for 100 ns.

Molecular Docking and Ligand-Bound Simulations. To study the binding mode and dynamics of PGS and CBZ bound to CYP3A4, we first employed molecular docking using Autodock 4.2[34,35] to probe potential binding sites for these drugs in the enzyme. Taking advantage of the MD simulation of membrane-bound CYP3A4 described above, we included a large number of snapshots taken from the 100 ns trajectory (in contrast to a single structure used in most docking studies) in our docking as described below. This approach allows us to take into the account the dynamics of the protein in the presence of the membrane and probe in our docking cavities and putative binding sites that only transiently arise during the simulations. The snapshots of membrane-bound CYP3A4 were taken from the MD trajectory at 1 ns intervals, resulting in 100 different snapshots, which were then used for docking of either PGS or CBZ.

Protein−ligand interactions were modeled with the Lamarckian genetic algorithm[34] with a grid box spanning the allosteric binding site region (near the F−F′ and G−G′ loops in CYP3A4) for both PGS and CBZ, and around the active site for CBZ. The top 10 docking poses for each snapshot and for each ligand (1000 poses for PGS and 1000 poses for CBZ) were collected for further analysis. The resulting docked structures were then clustered on the basis of their root-mean-square deviation (rmsd), using an rmsd cutoff of 2 Å, resulting in a total of five clusters for each ligand. For PGS in the allosteric binding site, the docked poses in which the substrate adopts an orientation similar to that of the crystal structure of substrate-bound CYP3A4[36] were chosen as starting positions for the MD simulations of ligand-bound systems. For CBZ in the allosteric site, the docking poses with the highest docking scores from the pool of the first four clusters were selected as starting positions for ligand-bound MD simulations. In the case of CBZ in the active site, the best docked pose (highest docking score) in each cluster was selected as initial positions for MD simulations. Two of the initial positions of CBZ were discarded on the basis of the distance between the sites of metabolism of the substrate (C10 and C11) and the heme iron (>6 Å), resulting in only three initial orientations for a single CBZ molecule in the active site. The resulting systems were minimized for 1000 steps and equilibrated for 100 ps while the heavy atoms of the protein backbone and the ligand were harmonically restrained (k = 1 kcal mol^{-1} Å^{-2}). This step was then followed by unrestrained, production simulations.

DOI: 10.1021/acs.biochem.5b00079
Biochemistry 2015, 54, 2227−2239

Simulations of substrates in the allosteric site were run each for 30−100 ns for CBZ and 100 ns for PGS. For a single CBZ in the active site, the production simulations were each 10−20 ns in duration.

To generate models for two CBZ molecules bound to CYP3A4, the general molecular docking approach was repeated employing snapshots from the single CBZ simulations where the distance between CBZ C10/C11 and the heme iron was <6 Å, resulting in 30 frames. In this case, each snapshot also included the first CBZ molecule, in addition to the protein. The resulting docked poses of the two CBZ molecules were clustered on the basis of the rmsd, with an rmsd cutoff of 2 Å. The best docked pose for each cluster was then selected as the initial configuration for additional MD simulations, resulting in four independent systems each with two CBZ molecules bound.

Molecular Dynamics (MD) Simulation Conditions and Protocols. MD simulations were performed using NAMD2,[37] utilizing the CHARMM36 force field with cMAP[38] corrections for the protein and CHARMM36[39] for lipids. Parameters for PGS were derived from available testosterone and cholesterol CHARMM parameters.[40,41] Parameters for CBZ were obtained by analogy[42,43] from the CHARMM General Force Field[39] and further optimized employing the Force Field Toolkit,[44] implemented in VMD.[45] The TIP3P model was used for water.[46] All simulations were performed as an *NPT* ensemble at 1.0 atm and 310 K, with a time step of 2 fs. Constant pressure was maintained using the Nosé−Hoover Langevin piston method,[47,48] and constant temperature was maintained by Langevin dynamics with a damping coefficient of 0.5 ps^{-1} applied to all atoms. Nonbonded interactions were cut off after 12 Å with a smoothing function applied after 10 Å. Bond distances involving hydrogen atoms were constrained using the SHAKE algorithm.[49] The particle mesh Ewald (PME) method[50] was used for long-range electrostatic calculations with a grid density of >1 $Å^{-3}$.

RESULTS

To understand the mechanism of activation of CYP3A4-mediated metabolism of one or both substrates in the mixture, we collected the spin shift titration data and steady-state kinetics of substrate turnover with PGS and CBZ separately, as well as in the mixed titration experiments as described in our earlier work on CYP3A4 heterotropic cooperativity.[25,31] All experiments were performed under identical conditions, allowing us to use the same set of binding constants in the analysis of multiple experiments.

Kinetics of PGS and CBZ Oxidation. The results of the spectral titration of CYP3A4 with PGS are shown in Figure 1 together with the rate of steady-state NADPH oxidation and the rate of product formation at various substrate concentrations. The spin shift titration and the rate of hydroxylation reveal pronounced apparent cooperativity with a sigmoidal concentration dependence. The rate of PGS hydroxylation reaches 16.6 min^{-1} at saturation, in agreement with earlier results.[8,51] Fitting with the Hill equation shows an n_H of 1.7, also similar to earlier reports for CYP3A4 with PGS.[51] The rate of NADPH consumption reaches a maximal value of 240 min^{-1} at 30 μM PGS and then slowly decreases at higher PGS concentrations to 160 min^{-1}. These observations are in a good agreement with our results obtained earlier for testosterone (TST) and ANF metabolism by CYP3A4 reconstituted in Nanodiscs.[24,25,31] Stepwise dissociation constants K_1, K_2, and K_3 were determined to be 7, 14, and 36 μM, respectively. This corresponds to an overall tighter binding but a progressive pattern similar to that resolved earlier in our work with TST (which had values of 19, 37, and 56 μM, respectively[24]). The only difference between the parameters resolved for TST and PGS is a moderate spin shift (37%) obtained for the second binding event with PGS (Table 1) as compared with an almost completely high-spin state obtained for TST.[24] The apparent K_m for PGS hydroxylation was estimated from the fitting curve as the concentration of substrate at which $v = V_{max}/2$ for the purpose of a proper choice of molar stoichiometry of PGS and CBZ in the mixed substrate experiments. For PGS, the value of K_m estimated from the fit is 16 μM (Figure 1).

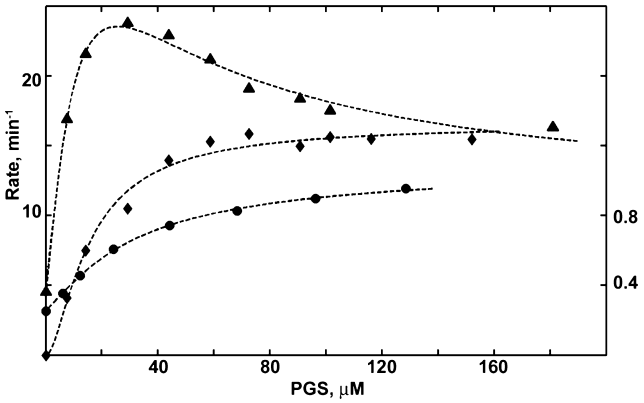

Figure 1. Results of the global analysis for PGS hydroxylation by CYP3A4. The spin shift titration (●, right axis), steady state rate of NADPH oxidation (▲, left axis), and product formation rates (◆, left axis) measured at various substrate concentrations are globally fit to the stepwise binding scheme as described in Experimental Procedures. The absolute values of experimentally measured rates and the percentage of high-spin shift were normalized for fitting (NADPH rate divided by 10 and fraction of high spin multiplied by 10) to ensure the same statistical weight of contributions from three different experimental data sets to the globally fitted parameters that are listed in Table 1.

The results obtained with pure CBZ as a substrate are shown in Figure 2. The NADPH oxidation rate reaches a maximal value of 123 min^{-1} at 200 μM CBZ and then decreases at higher substrate concentrations. The same effect is observed with PGS, although the absolute rate of NADPH consumption with CBZ is 2 times lower at maximum. In contrast, the rate of product formation is low at 200−300 μM CBZ and reaches its maximal value only at concentrations of ≥500 μM. The dependence of the spin shift on concentration is much smaller than with the steroids, as mentioned earlier, but also reveals the same sigmoidal shape with the lag at low CBZ concentrations. Moderate positive cooperativity with Hill coefficients from 1.4 to 2.1 was also reported in a recent study of CBZ metabolism by recombinant wild-type CYP3A4 and several mutants.[29]

All data for CBZ shown in Figure 2 were simultaneously fit using the same three-site binding scheme used for the steroid substrates.[24] The results of this fit are plotted in Figure 2 as smooth curves, and calculated parameters are listed in Table 1. According to the fitted parameters, the product formation rate is negligible when only one CBZ molecule is bound to CYP3A4. The absence of the product from the first binding intermediate was also reported for CBZ epoxidation by CYP3A4 in human liver microsomes[52,53] and in insect cells microsomes.[17,54] Binding of the second substrate molecule

DOI: 10.1021/acs.biochem.5b00079
Biochemistry 2015, 54, 2227−2239

Table 1. Parameters Derived from Single-Substrate Global Analyses[a]

	PGS		
	K_d = 7 μM (4.4–10.4)	K_d = 14 μM (11–18)	K_d = 36 μM (27–48)
	high-spin fraction	NADPH rate (nmol nmol^{-1} min^{-1})	product formation rate (nmol nmol^{-1} min^{-1})
[**00**]	21	44	0
[**10**]	22 (25–40)	171 (126–220)	0 (0.01)
[**20**]	37 (26–47)	388 (343–450)	14.7 (13.8–15.8)
[**30**]	92 (88–97)	108 (100–114)	16.6 (16.3–16.9)
	CBZ		
	K_d = 100 μM (73–134)	K_d = 210 μM (113–340)	K_d = 570 μM (330–900)
	high-spin fraction	NADPH rate (nmol nmol^{-1} min^{-1})	product formation rate (nmol nmol^{-1} min^{-1})
[**00**]	21	41	0
[**01**]	22 (12–31)	195 (155–227)	0 (0.01)
[**02**]	22 (8–33)	124 (90–163)	1.7 (0.9–2.4)
[**03**]	59 (54–64)	56 (46–66)	3.0 (2.7–3.4)

[a]Confidence intervals shown in parentheses were calculated as described.[25]

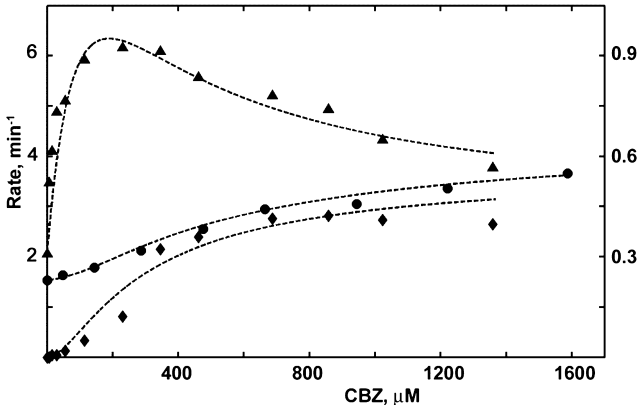

Figure 2. Results of the global analysis for CBZ epoxidation by CYP3A4. The spin shift titration (●, right axis), steady state rate of NADPH oxidation (▲, left axis), and product formation rates (◆, left axis) measured at various substrate concentrations are globally fit to the stepwise binding scheme as described in Experimental Procedures. The absolute values of experimentally measured rates and the percentage of high-spin shift were normalized for fitting (NADPH rate divided by 10 and fraction of high spin multiplied by 10) to ensure the same statistical weight of contributions from three different experimental data sets to the globally fit parameters that are listed in Table 1.

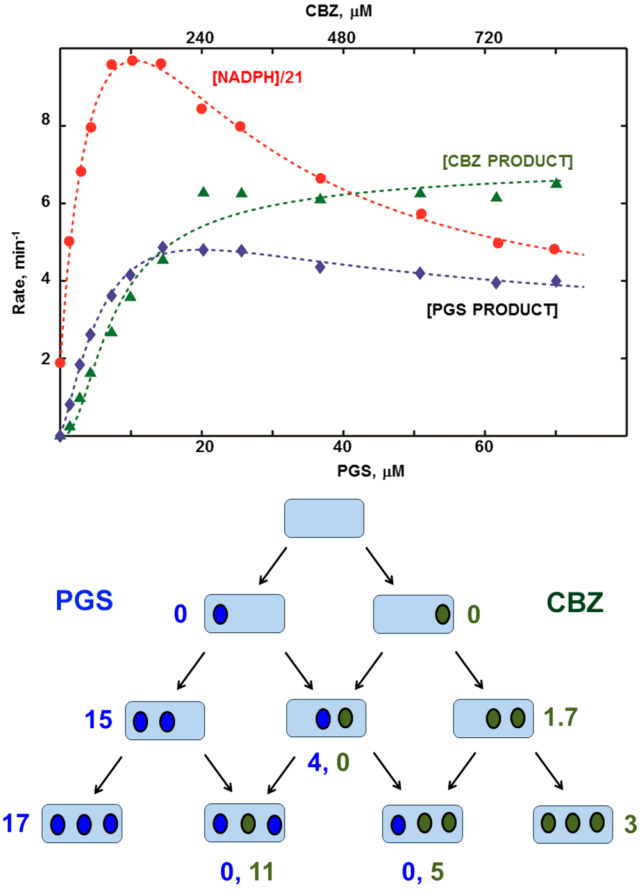

Figure 3. NADPH consumption rate and product forming rates (top) for PGS and CBZ observed using the mixture of PGS and CBZ at a 1:12 molar ratio. PGS concentrations are shown at the bottom and corresponding CBZ concentrations at the top. Rates (min^{-1}) of product formation (bottom image) for all 10 binding intermediates with results for PGS hydroxylation colored blue and those for CBZ epoxidation green.

triggers productive metabolism with an estimated rate of 1.7 min^{-1}, which increases to 3 min^{-1} after the third binding event. This pattern is different from that observed with TST and PGS, where the maximal hydroxylation rate has already been achieved after the second substrate binding, and the third substrate binding resulted in only better coupling but not faster catalysis. A similar difference is seen in the high-spin fraction of the [**20**] intermediate, where the CYP3A4 with two PGS molecules bound exhibits a substantial spin shift, while binding of two CBZ molecules still does not cause any spin shift.

Asymmetric Heterotropic Effect in PGS/CBZ Mixtures. The results of experiments with the mixture of CBZ and PGS are shown in Figure 3. The molar ratio of two substrates (12:1 CBZ:PGS) was selected on the basis of the apparent averaged K_m values determined from the midpoints of the fitting curves for product formation rates for pure substrates in Figures 1 and 2. The absolute rate of NADPH consumption at maximum, and the shape of its dependence on the substrate concentration, are very similar to those observed with pure CBZ (Figure 2). However, the maximal rate is reached already at 10 μM PGS and 120 μM CBZ, i.e., at significantly lower concentrations compared to those when only a single substrate is present. In addition, significantly different values of the product formation rates are observed for both PGS and CBZ. For PGS, the

DOI: 10.1021/acs.biochem.5b00079
Biochemistry 2015, 54, 2227–2239

Table 2. Parameters Derived from the Global Analysis of the Mixed Substrate Experiments[a]

	$\Delta\Delta G_{coop}$ = −1 kcal/mol (−1.2 to −0.8)	$\Delta\Delta G_{coop}$ = 0.7 kcal/mol (0.55−0.9)	$\Delta\Delta G_{coop}$ = 0.3 kcal/mol (0.2−0.45)
	NADPH rate (nmol nmol^{-1} min^{-1})	PGS product rate (nmol nmol^{-1} min^{-1})	CBZ product rate (nmol nmol^{-1} min^{-1})
[**11**]	410 (387−434)	4 (3.7−4.2)	0 (0.01)
[**21**]	120 (106−134)	0 (0.02)	11 (9.8−12.2)
[**12**]	128 (82−166)	0 (0.01)	4.5 (2.0−6.0)

[a]Confidence intervals shown in parentheses were calculated as described.[25]

maximal product formation rate (5 min^{-1}) is reached at 18−20 μM PGS, with the subsequent decrease to 4 min^{-1} at 60 μM and higher PGS concentrations. This is 4 times slower than the maximal rate observed with pure PGS, indicating substantial inhibition of PGS hydroxylation in the presence of CBZ. At the same time, the rate of CBZ epoxidation reaches a maximal value of 6 min^{-1} at 240 μM CBZ and then remains approximately the same up to 800 μM CBZ. This rate is 2 times higher than the rate of 3 min^{-1} observed with pure CBZ, meaning significant activation of CBZ metabolism in the presence of PGS. Note that all rate values are calculated per total CYP3A4, which metabolizes both substrates in the mixture, so the actual activation for CBZ and inhibition for PGS are even more pronounced. Importantly, this activation is seen with monomeric CYP3A4.

The global fitting of these experimental results has been performed using fixed parameters for homotropic parts of Scheme 1, which were determined in separate experiments (Table 1). Parameters evaluated for the mixed intermediates are listed in Table 2. As evident from the results shown in Figure 3, PGS hydroxylation is observed at the relatively slow rate of 4 min^{-1} only from the [**11**] intermediate, where one PGS and one CBZ molecule are bound simultaneously to the CYP3A4 monomer. In addition, formation of [**11**] is favorable by the additional $\Delta\Delta G_{coop}$ of approximately 1 kcal/mol, resulting in a 5-fold larger population of this intermediate as compared with [**20**] and [**02**]. This fact partly explains the steep increase in the rates of NADPH oxidation and product formation at relatively low concentrations of substrates seen in Figure 3.

Neither intermediate [**21**] nor intermediate [**12**] shows any measurable product formation for PGS, indicating predominant positioning of CBZ at the productive site near the heme iron in these intermediates. The product formation rates for CBZ obtained for these intermediates (11 and 4.5 min^{-1} for [**21**] and [**12**], respectively) are significantly higher than 3 min^{-1} for CBZ alone, revealing these faster rates as the main source of activation of CBZ epoxidation in the presence of PGS. Interestingly, no CBZ product is formed in the [**11**] intermediate. This may be explained either by preferential PGS positioning at the productive site in this intermediate or by the low efficiency of productive CBZ catalysis in [**11**], if both PGS and CBZ have access to the catalytically active iron−oxo intermediate. Taking into account the very high rate of NADPH oxidation (410 min^{-1}) and the low rate of PGS hydroxylation (4 min^{-1}) obtained for the [**11**] intermediate (Table 2), we found the second explanation seems to be more consistent with all experimental data, although no definite conclusion can be made without site-specific structural information, which is currently unavailable. As a result, CBZ epoxidation is significantly accelerated in the presence of PGS, while PGS hydroxylation is strongly inhibited. This asymmetric heterotropic effect can be explained only by an uneven distribution of two substrates between the productive binding site close to the heme iron and the unproductive peripheral binding sites.

Dynamics of PGS and CBZ in the Allosteric Site of CYP3A4. To explore the effects of multiple-ligand binding and gain insight into the structural basis of heterotropic cooperativity in CYP3A4, we performed several MD simulations of the enzyme in the presence of PGS or CBZ at different binding sites. It has been suggested that the mechanism of cooperativity of CYP3A4 is regulated by the binding of a ligand to a peripheral binding site.[10,36,55−57] The binding of a substrate in the periphery of CYP3A4 might trigger a conformational change necessary to facilitate the cooperative behavior of the enzyme. In this regard, experimental structural studies have identified a peripheral binding site in the proximity of the F−G region of the enzyme,[36,55] with X-ray crystal structures revealing PGS binding at this site. In the membrane-bound form of CYP3A4, the peripheral binding site is located in a region that interacts with the membrane.[33,58] Given the partitioning of steroids in the membrane[59] in a region located between the headgroup and lipid tails, it is likely that a substrate can be recruited by the enzyme and bind to this peripheral site, resulting in allosteric modulation of CYP3A4 function.

To study the dynamics of PGS in the allosteric binding site of CYP3A4 in the presence of a lipid bilayer, we performed three independent MD simulations starting from docked poses where the ligand has a conformation similar to that of the available crystal structure of PGS-bound CYP3A4[36] (Figure 4). Similarly, we executed four independent simulations with CBZ docked in the allosteric binding site. Because there is no structural information about binding of CBZ to this allosteric site, we tested four different docked poses for CBZ, one in each simulation (Figure 5). In the resulting docked poses, PGS and CBZ are packed in the vicinity of the hydrophobic side chains in the allosteric binding site. During the simulations, PGS maintains its contacts with hydrophobic side chains located in this region, particularly with Phe-219 and Phe-220, while forming additional transient contacts with Leu-211, Asp-217, and Arg-243. In the case of CBZ, the substrate detached from the enzyme in three of the four simulations, as quantified by its rmsd evolution (Figure 5). In the single simulation in which CBZ remains bound to the enzyme, it is stabilized by interactions between its carbonyl oxygen and the backbone amide group of Leu-211 and between its amine nitrogen and backbone carbonyl oxygen atoms of Leu-211 and Val-240 (Figure 5).

Interestingly, the presence of PGS in the allosteric binding site induces a change in the orientation of the Phe-213 side chain, located in the F−F′ loop (Figure 4). In the absence of the substrate, Phe-213 is located closer to the productive binding site (active site), with its side chain pointing toward the heme and away from the membrane. In this orientation, the average distance between Phe-213 and the heme is 14.7 Å. In the simulations in which PGS is bound to CYP3A4, a transient change in the orientation of Phe-213 is observed. In these cases,

DOI: 10.1021/acs.biochem.5b00079
Biochemistry 2015, 54, 2227−2239

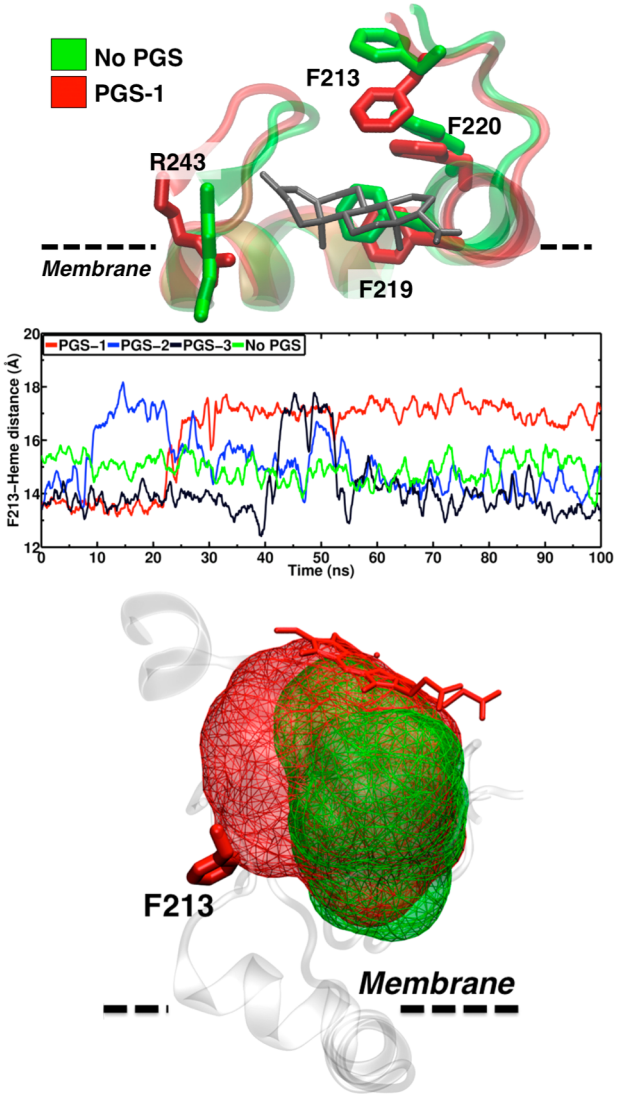

Figure 4. Dynamics of PGS in the allosteric binding site of CYP3A4. Representative snapshots (top) of the conformation of the F−G region of CYP3A4 for both substrate-free (green) and PGS-bound simulations (red). Side chains of residues interacting with PGS are shown as sticks in their respective colors. PGS is shown as gray sticks. Time series (middle) of the center of mass (COM) distance between the Phe-213 side chain and the heme. The average distance for the substrate-free simulation over 100 ns is 14.7 Å. Change in the active site volume (bottom) resulting from the displacement of Phe-213 from the active site. The Phe-213 side chain and the heme moiety are shown as red sticks. The volume was calculated using the program "mdpocket".[27]

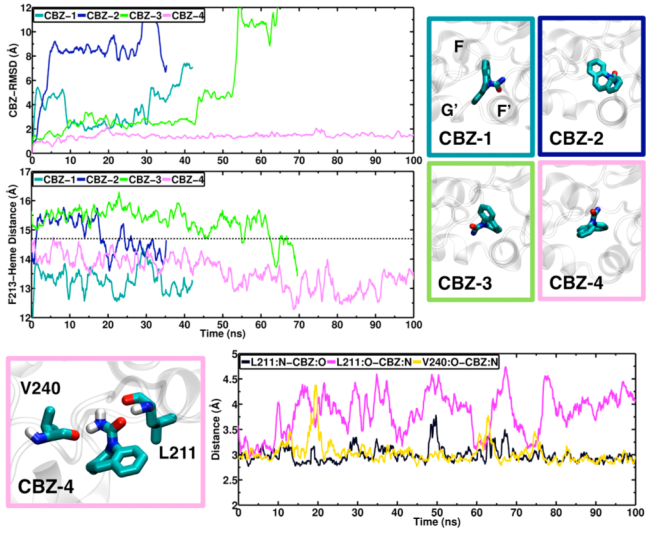

Figure 5. Dynamics of CBZ in the allosteric binding site of CBZ. Snapshots (top left) of the four different orientations of CBZ in the peripheral binding site probed with MD simulations. Time series (top right) of the rmsd of CBZ and the COM distance between the Phe-213 side chain and the heme for each simulation. The average distance for the 100 ns substrate-free simulation is 14.7 Å (dashed line). Snapshot (bottom left) of interactions of CBZ with residues Leu-211 and Val-240, obtained from system CBZ-4. CBZ and residues Leu-211 and Val-240 are shown as sticks. Time series (bottom right) of the distance between interacting elements of CBZ and Leu-211 and Val-240.

the Phe-213 side chain flips out of the active site and packs against PGS, resulting in an increase of ∼4 Å in the distance between its side chain and the heme. In contrast, in the CBZ simulations, Phe-213 remains pointing toward the active site, with the distances between the side chain and heme being ∼14 Å, similar to that of the substrate-free simulation, even in the simulation where CBZ remains bound to CYP3A4 (Figure 5). This local conformational change induced by PGS favors an increase in the volume of the CYP3A4 active site, from 675 $Å^3$ in the absence of the substrate to 990 $Å^3$ when PGS is present in the allosteric binding site. The relevance of Phe-213 in cooperativity has been observed experimentally, where mutation of this residue results in the reduced cooperativity of CYP3A4[60] and decreased level of stimulation by ANF.[8] In the context of the membrane, our simulations suggest that Phe-213 is important for modulating cooperativity by allowing an increase in the volume of the active site, therefore facilitating the binding of other substrates in the productive site of CYP3A4.

Dynamics of CBZ in the Active Site. The active site of CYP3A4 is capable of accommodating more than one substrate molecule, as suggested by X-ray structures in which two ketoconazole[61] or ritonavir[62,63] molecules were found in the active site. To study the dynamics of CBZ in the active site, we have performed several independent simulations in which one or two CBZ molecules are located in the active site. Although several binding modes of CBZ based on molecular docking have been previously proposed,[64] none of the previous studies except ref 29 took into account the dynamics of the binding site and the substrate. Therefore, to take into account different potential orientations of the substrate in the active site, we performed three independent simulations, each starting from one of the three most representative docked poses of a single CBZ molecule in the active site (Figure 6). During these simulations, CBZ is significantly displaced from its initial position in the active site, as shown by the distances between the heme iron and C10 and C11 of CBZ (Figure 6). For example, in system CBZ-3, the molecule transiently approaches the heme (heme iron−C10 or −C11 distances of <5 Å), while in systems CBZ-1 and CBZ-3, the molecule gradually drifts away from its initial position and from the heme. Together, these simulations suggest that it may be difficult for a single CBZ molecule to find a stable position and orientation that would facilitate its oxidation.

Starting from the snapshots obtained from single-CBZ simulations, and employing molecular docking, we also

DOI: 10.1021/acs.biochem.5b00079
Biochemistry 2015, 54, 2227−2239

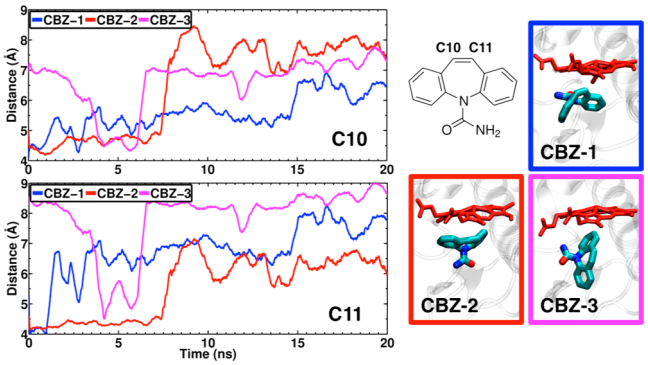

Figure 6. Dynamics of a single CBZ in the active site of CYP3A4. Snapshots (right) of the three different orientations of CBZ in the active site probed with MD simulations. The structure of CBZ is also shown, indicating its sites of metabolism, C10 and C11. CBZ is shown as sticks. The heme moiety is shown as a red stick. Time series (left) of the distance between C10 and C11 of CBZ and the heme iron atom.

generated membrane-bound models of CYP3A4 with two CBZ molecules in the active site. For this condition, we tested four different initial configurations. In these systems, the CBZ molecule that is closer to the heme remains in its position during the simulations, with C10− and C11−heme iron distances of ∼5 Å (Figure 7). This observation suggests that the presence of a second CBZ molecule could favor the epoxidation of the first molecule by keeping it in the proximity of the heme. Moreover, the simulations reveal that some of the tested two-CBZ configurations favor the transient motion of Phe-213 out of the active site (Figure 7). This is particularly evident in system CBZ-2, where the distance between the Phe-213 side chain and the heme remains above the average of 14.7 Å observed in the substrate-free simulation. In this case, the Phe-213 side chain is displaced from the active site, allowing the second CBZ molecule to occupy its position and contact Phe-241 and Phe-304. The observed displacement of Phe-213 in this case suggests that the binding of two or more substrates in the active site of CYP3A4 might be facilitated by the binding of another substrate, such as PGS in our case, to the peripheral binding site. Therefore, these simulations provide some structural insight into the role of the different substrates in the mechanism of cooperativity of CYP3A4.

DISCUSSION

In this work, we provide a detailed analysis of heterotropic interactions between two substrates and monomeric CYP3A4 incorporated in POPC Nanodiscs. Using a reconstituted system with CPR, we measured the steady-state rates of NADPH oxidation and product formation with CBZ and PGS as a function of substrate concentration in both homotropic (with individual substrates) and heterotropic (with a substrate mixture at a constant molar ratio) titration experiments. In addition, we performed type I spin shift titration experiments with pure substrates and their mixture under identical conditions. Simultaneous analysis of multiple experimental data sets allows us to decipher the stepwise substrate binding constants and fractional contributions from the binding intermediates with one, two, or three bound substrate molecules to the overall experimentally measured metabolic parameters of CYP3A4 in Nanodiscs (results listed in Tables 1 and 2). The resolved parameters provide a detailed picture of cooperative properties of CYP3A4, similar to the mechanism of

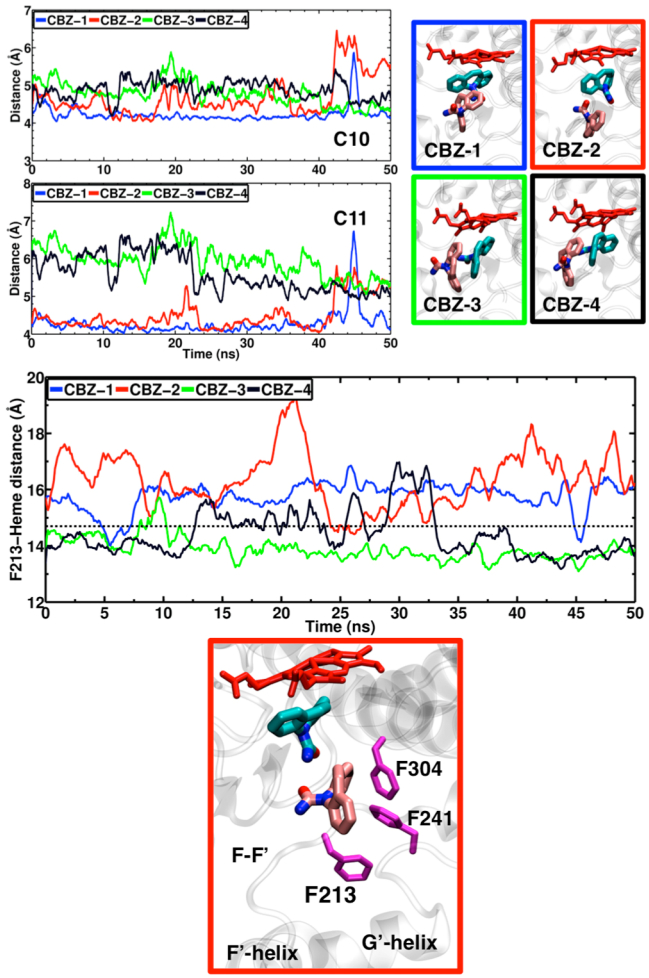

Figure 7. Two CBZ molecules in active site of CYP3A4. Snapshots (top right) of the four different configurations of two CBZ molecules in the active site probed with MD simulations. CBZ molecules are shown as sticks colored cyan (first molecule) and pink (second molecule). Time series (top left) of the distance between C10 and C11 of the first CBZ and the heme iron atom. Time series (middle) of the COM distance between the Phe-213 side chain and the heme. The average distance for the 100 ns substrate-free simulation is 14.7 Å (dashed line). Snapshot (bottom) showing a representative configuration from system CBZ-2 in which Phe-213 is displaced from the active site. Phe-213, Phe-241, and Phe-304 are shown as magenta sticks.

homotropic cooperativity with TST as a substrate, as described previously.[24]

The direct manifestation of heterotropic interactions between two different substrates bound to one CYP3A4 monomer is determined by the contribution of three mixed intermediates, i.e., [**11**], [**21**], and [**12**] in Scheme 1, to the overall observed functional properties of the enzyme. This contribution depends both on the functional properties of these intermediates and on their populations. The first factor depends on the probability of a particular substrate occupying the productive site, which can be different for a given intermediate. For instance, in [**11**], one of the substrates may be predominantly bound near the heme iron, while another may be bound at the remote nonproductive site. In addition, the rate of product formation depends on the efficiency of the catalytic step, or coupling at this configuration, which also can vary significantly, even if both substrates occupy the productive site

DOI: 10.1021/acs.biochem.5b00079
Biochemistry 2015, 54, 2227−2239

with the same probability. The second factor, the relative population of a given binding intermediate, depends on the corresponding stoichiometric binding constants, including possible allosteric or cooperative interactions between substrate molecules, and, obviously, on the absolute concentrations of both substrates. Clearly, if simultaneous binding of two types of substrates to one CYP3A4 molecule is strongly unfavorable, then the overall functional heterotropic effects will be weak, because the relative population of the mixed intermediates will be also low, and their contribution will be small. In the opposite scenario, when the population of mixed intermediates is high because of a positive cooperative interaction between the two substrates, the behavior of the system will be determined by their functional properties, because they will dominate in the mixture. The experimental protocol and global analysis approach described in this study allows one to determine these binding constants and properties of the mixed binding intermediates and to understand the molecular mechanisms of heterotropic cooperativity in CYP3A4.

Comparison of the properties of homotropic binding intermediates [**20**] and [**02**] with those of [**11**] reveals a strong asymmetry in the latter case. While the rate of PGS hydroxylation is 14.7 min^{-1} at a NADPH consumption rate of 388 min^{-1} for [**20**], it drops to 4 min^{-1} in [**11**] with NADPH consumption being even faster (410 min^{-1}), yet no CBZ product is produced (Figure 3). This drop in the coupling ratio suggests a looser packing of both substrates when both substrates are in the binding cavity or a much weaker allosteric effect of CBZ on the PGS hydroxylation if CBZ binds at the remote nonproductive binding site (Figure 5). Although no site-specific structural information is currently available to allow one to distinguish between these two cases, useful information can be obtained from molecular modeling. For example, flexible docking of CBZ and TST in CYP3A4[26] suggested that the optimal positioning of TST in productive mode near the heme iron is consistent with positioning of CBZ in the substrate binding pocket between TST and the G−G′ loop near Cys-239. This result provides a reasonable explanation for the observed preferential PGS hydroxylation in the [**11**] intermediate. In addition, CBZ was found to bind covalently inside the substrate binding cavity after prolonged incubation in a functionally reconstituted mixture,[26] with concomitant moderate inactivation of the enzyme with respect to TST hydroxylation. Analogously, PGS hydroxylation in intermediate [**11**] is also slower than in [**20**] by a factor of 4 (Tables 1 and 2).

The reversal of substrate selectivity and activation of CBZ epoxidation observed in intermediates [**12**] and [**21**] indicates that PGS binding at the allosteric site changes the shape of the active site and favors placement of CBZ in the vicinity of the heme iron. The absence of PGS hydroxylation products from these intermediates strongly suggests PGS binding at the remote, nonproductive site, and minimal, if any, occupation of the heme active site. At the same time, the rate of CBZ epoxidation is 1.5−3.5 times higher in [**12**] and [**21**], highlighting the positive heterotropic effect of PGS on CBZ metabolism. NADPH oxidation rates measured for [**12**] and [**21**] are approximately the same, and both are 2.5 times higher than that for [**03**], indicating essentially no changes in the coupling ratio caused by the replacement of one or two CBZ molecules with PGS.

Dramatic acceleration of CBZ epoxidation in the presence of PGS is consistent with results reported by Houston and collaborators,[4] where 2−6-fold faster CBZ metabolism by CYP3A4 in the presence of a large excess of PGS or other steroids was observed using human liver microsomes and human hepatocytes. Because the rate observed in the presence of 100 μM PGS was directly compared to the rate of CBZ epoxidation observed at the same low concentration of this substrate, 5 μM,[4] activation can be attributed to intermediate [**21**], in which two PGS molecules and one CBZ molecule are bound to CYP3A4. Our results for state [**21**] with a CBZ metabolism rate of 11 min^{-1} and 4-fold acceleration compared to state [**03**] are in agreement with these earlier results[4,19] and provide the specific molecular assignment of the main binding intermediate responsible for the acceleration of CBZ metabolism in the presence of steroids. Importantly, we also observe this significant heterotropic activation of CBZ epoxidation with PGS as an effector in monomeric CYP3A4 in Nanodiscs, which allows us to rule out effects of oligomerization.

Overall, the results summarized in Table 2 show distinct patterns of metabolism of CBZ and PGS by CYP3A4 in the mixed intermediates, as compared to the homotropic experiments shown in Table 1. As discussed above, this difference is explained by preferential distribution of these two substrates between the productive and nonproductive sites, while binding to the latter results in significant allosteric effects, as confirmed by significant activation of CBZ epoxidation in [**21**] and [**12**]. In both these intermediates, the absence of the PGS product implies dominant binding of this substrate at nonproductive sites. MD simulations reported in this study suggest a structural mechanism explaining the observed synergy between PGS, found to bind between F−F′ and G−G′ helices, and activation of CBZ metabolism. As seen in Figure 4, PGS binding at this peripheral site results in the movement of the Phe-213 side chain out of the binding pocket and a concomitant increase in the volume of the substrate binding cavity. Moreover, MD simulation of two CBZ molecules inside the substrate binding pocket (Figure 7) reveals the same outward movement of Phe-213 to provide the necessary space for the second CBZ molecule to bind. This striking similarity of conformational changes involving Phe-213 and its neighboring residues in response to PGS binding at the allosteric site and those involved in accommodating two CBZ molecules inside the substrate binding cavity in a productive position provides a possible molecular mechanism of allosteric communication between the remote and productive binding sites in CYP3A4.

The experimental and simulation results described herein provide a basis for the general picture of cooperative interactions between two different substrates in monomeric CYP3A4. Up to three substrate molecules of moderate size can bind simultaneously to one CYP3A4 molecule in the Nanodisc bilayer. However, at any given moment, only one substrate molecule can be positioned closest to the catalytically active iron−oxygen intermediate for the oxidative transformation. This position may be termed the productive site (P-site). The remote site that is not productive and spectroscopically silent during the spectral binding experiments was suggested to have allosteric properties (A-site), because binding of substrate to this site can result in perturbation of the functional properties of cytochrome P450, such as substrate positioning, regiospecificity of catalysis,[13,65−67] rate of autoxidation,[22] and overall coupling.[24,25] On the basis of the functional properties of site-specific mutants,[8,51,68] the X-ray structure of PGS-bound CYP3A4,[36] and fluorescent probes of its location,[10,55,69] the remote site is thought to be located at the surface of the protein

DOI: 10.1021/acs.biochem.5b00079
Biochemistry 2015, 54, 2227−2239

in the region between the F−F′ and G−G′ loops at the membrane interface.[58]

Many of the substrates can interact with both the productive and allosteric sites with or without pronounced cooperativity of binding. However, the observable properties, i.e., spectroscopic response and the product turnover rate, strongly depend on the specific positioning of the bound substrate. On the basis of differential binding affinities for the productive and remote allosteric sites, all substrates of CYP3A4 can be roughly separated into two classes, P-type and A-type. The presence of two substrate molecules inside the substrate binding pocket can place one near the heme iron for metabolism, and the second in an unfavorable position to interact with the iron−oxo intermediate itself while in direct steric contact with the first. Examples of the latter type of binding can be seen in the X-ray structures of CYP3A4 with ketoconazole[61] and analogues of ritonavir,[62,63] and also in P450eryF with androstenedione,[70] CYP158A2 with flavioline,[71] and CYP2B4 and CYP2B6 structures.[72,73] In addition, dramatic acceleration of hydroxylation of small hydrocarbons and benzene by CYP102A1 has been demonstrated in the presence of a "decoy" effector molecule of perfluorodecanoic acid, which filled the active site cavity and stabilized binding of small hydrocarbon substrates near the active iron−oxygen intermediate.[74,75] Cooperativity seems to be much more common for cytochromes P450 than we realized in the past. Biochemical analyses have indicated homotropic cooperativity in substrate binding by CYP392E10 from spider mite *Tetranychus urticae*[76] and heterotropic cooperativity in DDT metabolism by the insect P450 (CYP6M2 in *Anopheles gambiae*),[77] which is similar to what is reported for CYP3A4 and other human cytochromes P450, such as CYP11A1[78] and CYP46A1.[79]

In the mixture of A-type and P-type substrates at a 1:1 ratio, normalized to the concentration of each needed for the half-maximal spectral response or activity, the actual sites occupied by the two different substrates are likely to be asymmetric, with an A-type substrate showing a preference for A-site association, and a P-type substrate preferentially binding inside the substrate binding cavity. The magnitude of such competition for the active site between P-type and A-type substrates will also depend on the details of their mutual packing in the substrate binding pocket and the preferential positioning of one close to the iron−oxygen catalytic intermediate.

The presence of an allosteric site at the membrane interface suggests a potentially significant variation between experimentally determined drug−drug interactions with P450 enzymes when either incorporated into the lipid bilayer or detergent-solubilized systems.[78] This may be an important factor for the proper choice of an *in vitro* system for P450 activity studies in reconstituted systems. For the evaluation of potential drug−drug interactions between two or more substrates, the presence of the bilayer may be critically important. For analysis of unknown mixtures of several P450s using substrate cocktails,[80] the results may turn out different compared to those of a single P450 tested using only a single substrate, as other compounds may also serve as allosteric effectors. In cases in which there are pronounced interactions between P450 monomers resulting in the formation of P450 oligomers, it has been suggested that this protein−protein interface may involve the allosteric A-site.[10] If correct, interactions with A-type substrates could alter the monomer−oligomer equilibrium and the functional properties of oligomers. A role for oligomerization in the observed cooperativity of CYP3A4 was reviewed by Davydov and Halpert[81,82] and updated in their recent papers.[10,57] As these authors pointed out,[10,57] a significant fraction of P450 enzymes present in oligomers cannot interact with CPR and therefore may be not functional. Interactions with substrates and effectors can result in the redistribution of cytochromes P450 between functional and nonfunctional forms and thus play an important regulatory role. Further elucidations of mechanistic behavior of oligomeric CYP3A4 and other P450 enzymes outlined in refs 10 and 57 need to be based on a detailed understanding of modulation of the functional properties of monomeric CYP3A4 provided by oligomerization. Our results clearly demonstrate that even monomeric CYP3A4 in a membrane can display complex activation and allosteric responses.

In conclusion, we describe the results of experimental and computational studies of heterotropic interactions between two substrates of CYP3A4. Different properties of PGS and CBZ with respect to their binding affinity for productive and nonproductive allosteric sites give rise to strongly asymmetric mutual perturbation of their metabolic turnover catalyzed by monomeric CYP3A4, with strong activation of CBZ epoxidation and simultaneous inhibition of PGS hydroxylation in the mixed titration experiments. Using a global analysis, we have deconvoluted the partial contributions of the mixed binding intermediates into the overall observed rates of product formation and found a 1.5−3.5-fold acceleration of CBZ metabolism upon binding of one or two PGS molecules to the same CYP3A4 monomer. Importantly, our results obtained using CYP3A4 monomer in Nanodiscs are in very good agreement with the earlier results of Houston et al.[4,52] obtained with the same substrates using human liver microsomes and human hepatocytes, despite a recent claim that such heterotropic activation will not be reproducible in monomeric systems.[10] Results of MD simulations of PGS bound in the suggested allosteric remote site and one or two CBZ molecules bound inside the substrate binding cavity of CYP3A4 provide detailed insight into the possible conformational changes caused by these binding events. These conformational changes involving the side chains of several phenylalanine residues at the F−F′ and G−G′ loops are likely to give rise to the allosteric interactions between PGS binding outside of the binding cavity and CBZ binding inside the substrate binding pocket and explain the positive heterotropic cooperativity observed experimentally. Such a mechanism is expected to manifest itself with other substrates metabolized by CYP3A4, especially if their relative binding affinities with respect to the allosteric and productive sites are significantly different. Moreover, a similar mechanism may also apply to other membrane-bound eukaryotic cytochromes P450s, especially those with broad substrate specificities, because of the general similarity of their protein folds[83−85] and/or of their positioning in the membrane,[58] so that the F−F′ and G−G′ region is contacting the membrane surface and forms a pocket potentially suitable for accommodation of medium-sized hydrophobic molecules, such as endogenous steroids.

Three-site models for CYP3A4 have been suggested previously[27,28] to account for the rich variety of heterotropic effects observed in biochemical results before the solution of the first X-ray structure of a eukaryotic cytochrome P450 without any knowledge of the mode of incorporation of P450 into the membrane. We now have a more detailed picture of the possible modes of interactions of human cytochromes P450s with the membrane based on a large array of biophysical data and computational modeling.[33,58,83,86] However, high-

DOI: 10.1021/acs.biochem.5b00079
Biochemistry 2015, 54, 2227−2239

resolution structural information about the possible substrate binding sites for cytochromes P450 incorporated into the membrane is still not available. Current efforts to identify the location of allosteric site(s) and possible molecular mechanisms of cooperative interactions between nonproductive remote binding events and productive substrate binding to CYP3A4 based on a combination of biochemical and biophysical data with computational modeling suggest the mechanism involving several residues in the F−F′ and G−G′ loops, as illustrated in Figures 4 and 7, in agreement with earlier mutational studies.[8,51,68] Further studies employing site-specific structural methods together with specific mutations probing this site will improve our understanding of this mechanism in CYP3A4 and possibly other drug-metabolizing cytochromes P450s.

AUTHOR INFORMATION

Corresponding Author

*Department of Biochemistry, University of Illinois at Urbana-Champaign, 505 S. Goodwin Ave., Urbana, IL 61801. E-mail: s-sligar@illinois.edu. Telephone: (217) 244-9872. Fax: (217) 265-4073.

Funding

This work was supported by National Institutes of Health Grant R01-GM33775 to S.G.S., Grant R01-GM101048 to S.G.S. and E.T., and Grants R01-GM086749, U54-GM087519, and P41-GM104601 to E.T. All simulations were performed using XSEDE resources (Grant MCA06N060).

Notes

The authors declare no competing financial interest.

ABBREVIATIONS

ANF, α-naphthoflavone; CBZ, carbamazepine; COM, center of mass; CPR, cytochrome P450 reductase; MD, molecular dynamics; MSP, membrane scaffold protein; PGS, progesterone; POPC, palmitoyloleoylphosphatidylcholine; rmsd, root-mean-square deviation; TST, testosterone.

REFERENCES

(1) Evers, R., Dallas, S., Dickmann, L. J., Fahmi, O. A., Kenny, J. R., Kraynov, E., Nguyen, T., Patel, A. H., Slatter, J. G., and Zhang, L. (2013) Critical review of preclinical approaches to investigate cytochrome p450-mediated therapeutic protein drug-drug interactions and recommendations for best practices: a white paper. *Drug Metab. Dispos. 41*, 1598−1609.

(2) Shou, M., Grogan, J., Mancewicz, J. A., Krausz, K. W., Gonzalez, F. J., Gelboin, H. V., and Korzekwa, K. R. (1994) Activation of CYP3A4: Evidence for the simultaneous binding of two substrates in a cytochrome P450 active site. *Biochemistry 33*, 6450−6455.

(3) Ngui, J. S., Chen, Q., Shou, M., Wang, R. W., Stearns, R. A., Baillie, T. A., and Tang, W. (2001) In vitro stimulation of warfarin metabolism by quinidine: Increases in the formation of 4′- and 10-hydroxywarfarin. *Drug Metab. Dispos. 29*, 877−886.

(4) Henshall, J., Galetin, A., Harrison, A., and Houston, J. B. (2008) Comparative analysis of CYP3A heteroactivation by steroid hormones and flavonoids in different in vitro systems and potential in vivo implications. *Drug Metab. Dispos. 36*, 1332−1340.

(5) Blobaum, A. L., Bridges, T. M., Byers, F. W., Turlington, M. L., Mattmann, M. E., Morrison, R. D., Mackie, C., Lavreysen, H., Bartolome, J. M., MacDonald, G. J., Steckler, T., Jones, C. K., Niswender, C. M., Conn, P. J., Lindsley, C. W., Stauffer, S. R., and Daniels, J. S. (2013) Heterotropic activation of the midazolam hydroxylase activity of CYP3A by a positive allosteric modulator of mGlu5: In vitro to in vivo translation and potential impact on clinically relevant drug-drug interactions. *Drug Metab. Dispos. 41*, 2066−2075.

(6) Emoto, C., and Iwasaki, K. (2006) Enzymic characteristics of CYP3A5 and CYP3A4: A comparison of in vitro kinetic and drug-drug interaction patterns. *Xenobiotica 36*, 219−233.

(7) Shou, M., Dai, R., Cui, D., Korzekwa, K. R., Baillie, T. A., and Rushmore, T. H. (2001) A kinetic model for the metabolic interaction of two substrates at the active site of cytochrome P450 3A4. *J. Biol. Chem. 276*, 2256−2262.

(8) Domanski, T. L., He, Y.-A., Khan, K. K., Roussel, F., Wang, Q., and Halpert, J. R. (2001) Phenylalanine and Tryptophan Scanning Mutagenesis of CYP3A4 Substrate Recognition Site Residues and Effect on Substrate Oxidation and Cooperativity. *Biochemistry 40*, 10150−10160.

(9) Woods, C. M., Fernandez, C., Kunze, K. L., and Atkins, W. M. (2011) Allosteric activation of cytochrome P450 3A4 by α-naphthoflavone: Branch point regulation revealed by isotope dilution analysis. *Biochemistry 50*, 10041−10051.

(10) Davydov, D. R., Davydova, N. Y., Sineva, E. V., Kufareva, I., and Halpert, J. R. (2013) Pivotal role of P450-P450 interactions in CYP3A4 allostery: The case of α-naphthoflavone. *Biochem. J. 453*, 219−230.

(11) Walzer, M., Bekersky, I., Blum, R. A., and Tolbert, D. (2012) Pharmacokinetic drug interactions between clobazam and drugs metabolized by cytochrome P450 isoenzymes. *Pharmacotherapy 32*, 340−353.

(12) Parrish, R. H., Pazdur, D. E., and O'Donnell, P. J. (2006) Effect of carbamazepine initiation and discontinuation on antithrombotic control in a patient receiving warfarin: Case report and review of the literature. *Pharmacotherapy 26*, 1650−1653.

(13) Roberts, A. G., Yang, J., Halpert, J. R., Nelson, S. D., Thummel, K. T., and Atkins, W. M. (2011) The structural basis for homotropic and heterotropic cooperativity of midazolam metabolism by human cytochrome P450 3A4. *Biochemistry 50*, 10804−10818.

(14) Konishi, H., Tanaka, K., Minouchi, T., and Yamaji, A. (2004) Urinary 6β-hydroxycortisol/17-hydroxycorticosteroids ratio as a measure of hepatic CYP3A4 capacity after enzyme induction. *Ann. Clin. Biochem. 41*, 335−337.

(15) Ohno, Y., Hisaka, A., Ueno, M., and Suzuki, H. (2008) General framework for the prediction of oral drug interactions caused by CYP3A4 induction from in vivo information. *Clin. Pharmacokinet. 47*, 669−680.

(16) Spina, E., Pisani, F., and Perucca, E. (1996) Clinically significant pharmacokinetic drug interactions with carbamazepine. An update. *Clin. Pharmacokinet. 31*, 198−214.

(17) Nakamura, H., Torimoto, N., Ishii, I., Ariyoshi, N., Nakasa, H., Ohmori, S., and Kitada, M. (2003) CYP3A4 and CYP3A7-mediated carbamazepine 10,11-epoxidation are activated by differential endogenous steroids. *Drug Metab. Dispos. 31*, 432−438.

(18) Kerr, B. M., Thummel, K. E., Wurden, C. J., Klein, S. M., Kroetz, D. L., Gonzalez, F. J., and Levy, R. H. (1994) Human liver carbamazepine metabolism. Role of CYP3A4 and CYP2C8 in 10,11-epoxide formation. *Biochem. Pharmacol. 47*, 1969−1979.

(19) Egnell, A.-C., Houston, J. B., and Boyer, C. S. (2005) Predictive models of CYP3A4 heteroactivation: In vitro-in vivo scaling and pharmacophore modeling. *J. Pharmacol. Exp. Ther. 312*, 926−937.

(20) Denisov, I. G., Grinkova, Y. V., Baas, B. J., and Sligar, S. G. (2006) The ferrous-dioxygen intermediate in human cytochrome P450 3A4: Substrate dependence of formation of decay kinetics. *J. Biol. Chem. 281*, 23313−23318.

(21) Denisov, I. G., Grinkova, Y. V., Lazarides, A. A., and Sligar, S. G. (2004) Directed self-assembly of monodisperse phospholipid bilayer Nanodiscs with controlled size. *J. Am. Chem. Soc. 126*, 3477−3487.

(22) Denisov, I. G., Grinkova, Y. V., McLean, M. A., and Sligar, S. G. (2007) The one-electron autoxidation of human cytochrome P450 3A4. *J. Biol. Chem. 282*, 26865−26873.

(23) Grinkova, Y. V., Denisov, I. G., and Sligar, S. G. (2010) Functional reconstitution of monomeric CYP3A4 with multiple cytochrome P450 reductase molecules in Nanodiscs. *Biochem. Biophys. Res. Commun. 398*, 194−198.

DOI: 10.1021/acs.biochem.5b00079
Biochemistry 2015, 54, 2227−2239

(24) Denisov, I. G., Baas, B. J., Grinkova, Y. V., and Sligar, S. G. (2007) Cooperativity in cytochrome P450 3A4: Linkages in substrate binding, spin state, uncoupling, and product formation. *J. Biol. Chem. 282*, 7066−7076.
(25) Frank, D. J., Denisov, I. G., and Sligar, S. G. (2011) Analysis of heterotropic cooperativity in cytochrome P450 3A4 using α-naphthoflavone and testosterone. *J. Biol. Chem. 286*, 5540−5545.
(26) Kang, P., Liao, M., Wester, M. R., Leeder, J. S., Pearce, R. E., and Correia, M. A. (2008) CYP3A4-mediated carbamazepine (CBZ) metabolism: Formation of a covalent CBZ-CYP3A4 adduct and alteration of the enzyme kinetic profile. *Drug Metab. Dispos. 36*, 490−499.
(27) Domanski, T. L., He, Y.-A., Harlow, G. R., and Halpert, J. R. (2000) Dual role of human cytochrome P450 3A4 residue Phe-304 in substrate specificity and cooperativity. *J. Pharmacol. Exp. Ther. 293*, 585−591.
(28) Hosea, N. A., Miller, G. P., and Guengerich, F. P. (2000) Elucidation of Distinct Ligand Binding Sites for Cytochrome P450 3A4. *Biochemistry 39*, 5929−5939.
(29) Muller, C. S., Knehans, T., Davydov, D. R., Bounds, P. L., von Mandach, U., Halpert, J. R., Caflish, A., and Koppenol, W. H. (2015) Concurrent Cooperativity and Substrate Inhibition in the Epoxidation of Carbamazepine by Cytochrome P450 3A4 Active Site Mutants Inspired by Molecular Dynamics Simulations. *Biochemistry 54*, 711−721.
(30) Di Cera, E. (1995) *Thermodynamic Theory of Site-Specific Binding Processes in Biological Macromolecules*, Cambridge University Press, Cambridge, U.K.
(31) Frank, D. J., Denisov, I. G., and Sligar, S. G. (2009) Mixing apples and oranges: Analysis of heterotropic cooperativity in cytochrome P450 3A4. *Arch. Biochem. Biophys. 488*, 146−152.
(32) Yano, J. K., Wester, M. R., Schoch, G. A., Griffin, K. J., Stout, C. D., and Johnson, E. F. (2004) The structure of human microsomal cytochrome P450 3A4 determined by X-ray crystallography to 2.05-Å resolution. *J. Biol. Chem. 279*, 38091−38094.
(33) Baylon, J. L., Lenov, I. L., Sligar, S. G., and Tajkhorshid, E. (2013) Characterizing the membrane-bound state of cytochrome P450 3A4: Structure, depth of insertion, and orientation. *J. Am. Chem. Soc. 135*, 8542−8551.
(34) Morris, G. M., Goodsell, D. S., Halliday, R. S., Huey, R., Hart, W. E., Belew, R. K., and Olson, A. J. (1998) Automated docking using a Lamarckian genetic algorithm and an empirical binding free energy function. *J. Comput. Chem. 19*, 1639−1662.
(35) Morris, G. M., Huey, R., Lindstrom, W., Sanner, M. F., Belew, R. K., Goodsell, D. S., and Olson, A. J. (2009) AutoDock and AutoDockTools: Automated docking with selective receptor flexibility. *J. Comput. Chem. 30*, 2785−2791.
(36) Williams, P. A., Cosme, J., Vinkovic, D. M., Ward, A., Angove, H. C., Day, P. J., Vonrhein, C., Tickle, I. J., and Jhoti, H. (2004) Crystal structures of human cytochrome P450 3A4 bound to metyrapone and progesterone. *Science 305*, 683−686.
(37) Phillips, J. C., Braun, R., Wang, W., Gumbart, J., Tajkhorshid, E., Villa, E., Chipot, C., Skeel, R. D., Kale, L., and Schulten, K. (2005) Scalable molecular dynamics with NAMD. *J. Comput. Chem. 26*, 1781−1802.
(38) MacKerell, A. D., Jr., Feig, M., and Brooks, C. L., III (2004) Extending the treatment of backbone energetics in protein force fields: Limitations of gas-phase quantum mechanics in reproducing protein conformational distributions in molecular dynamics simulations. *J. Comput. Chem. 25*, 1400−1415.
(39) Vanommeslaeghe, K., Hatcher, E., Acharya, C., Kundu, S., Zhong, S., Shim, J., Darian, E., Guvench, O., Lopes, P., Vorobyov, I., and Mackerell, A. D., Jr. (2010) CHARMM general force field: A force field for drug-like molecules compatible with the CHARMM all-atom additive biological force fields. *J. Comput. Chem. 31*, 671−690.
(40) Fishelovitch, D., Shaik, S., Wolfson, H. J., and Nussinov, R. (2009) Theoretical Characterization of Substrate Access/Exit Channels in the Human Cytochrome P450 3A4 Enzyme: Involvement of Phenylalanine Residues in the Gating Mechanism. *J. Phys. Chem. B 113*, 13018−13025.
(41) Lim, J. B., Rogaski, B., and Klauda, J. B. (2012) Update of the Cholesterol Force Field Parameters in CHARMM. *J. Phys. Chem. B 116*, 203−210.
(42) Vanommeslaeghe, K., and MacKerell, A. D. (2012) Automation of the CHARMM General Force Field (CGenFF) I: Bond Perception and Atom Typing. *J. Chem. Inf. Model. 52*, 3144−3154.
(43) Vanommeslaeghe, K., Raman, E. P., and MacKerell, A. D. (2012) Automation of the CHARMM General Force Field (CGenFF) II: Assignment of Bonded Parameters and Partial Atomic Charges. *J. Chem. Inf. Model. 52*, 3155−3168.
(44) Mayne, C. G., Saam, J., Schulten, K., Tajkhorshid, E., and Gumbart, J. C. (2013) Rapid parameterization of small molecules using the force field toolkit. *J. Comput. Chem. 34*, 2757−2770.
(45) Humphrey, W., Dalke, A., and Schulten, K. (1996) VDM: Visual molecular dynamics. *J. Mol. Graphics 14*, 33−38.
(46) Jorgensen, W. L., Chandrasekhar, J., Madura, J. D., Impey, R. W., and Klein, M. L. (1983) Comparison of simple potential functions for simulating liquid water. *J. Chem. Phys. 79*, 926−935.
(47) Feller, S. E., Zhang, Y., Pastor, R. W., and Brooks, B. R. (1995) Constant pressure molecular dynamics simulation: The Langevin piston method. *J. Chem. Phys. 103*, 4613−4621.
(48) Martyna, G. J., Tobias, D. J., and Klein, M. L. (1994) Constant pressure molecular dynamics algorithms. *J. Chem. Phys. 101*, 4177−4189.
(49) Ryckaert, J. P., Ciccotti, G., and Berendsen, H. J. C. (1977) Numerical integration of the Cartesian equations of motion of a system with constraints: Molecular dynamics of n-alkanes. *J. Comput. Phys. 23*, 327−341.
(50) Darden, T., York, D., and Pedersen, L. (1993) Particle mesh Ewald: An N·log(N) method for Ewald sums in large systems. *J. Chem. Phys. 98*, 10089−10092.
(51) Harlow, G. R., and Halpert, J. R. (1998) Analysis of human cytochrome P450 3A4 cooperativity: Construction and characterization of a site-directed mutant that displays hyperbolic steroid hydroxylation kinetics. *Proc. Natl. Acad. Sci. U.S.A. 95*, 6636−6641.
(52) Egnell, A.-C., Houston, B., and Boyer, S. (2003) In vivo CYP3A4 heteroactivation is a possible mechanism for the drug interaction between felbamate and carbamazepine. *J. Pharmacol. Exp. Ther. 305*, 1251−1262.
(53) Nakamura, H., Nakasa, H., Ishii, I., Ariyoshi, N., Igarashi, T., Ohmori, S., and Kitada, M. (2002) Effects of endogenous steroids on CYP3A4-mediated drug metabolism by human liver microsomes. *Drug Metab. Dispos. 30*, 534−540.
(54) Maekawa, K., Yoshimura, T., Saito, Y., Fujimura, Y., Aohara, F., Emoto, C., Iwasaki, K., Hanioka, N., Narimatsu, S., Niwa, T., and Sawada, J. (2009) Functional characterization of CYP3A4.16: Catalytic activities toward midazolam and carbamazepine. *Xenobiotica 39*, 140−147.
(55) Davydov, D. R., Rumfeldt, J. A., Sineva, E. V., Fernando, H., Davydova, N. Y., and Halpert, J. R. (2012) Peripheral ligand-binding site in cytochrome P450 3A4 located with fluorescence resonance energy transfer (FRET). *J. Biol. Chem. 287*, 6797−6809.
(56) Denisov, I. G., and Sligar, S. G. (2012) A novel type of allosteric regulation: Functional cooperativity in monomeric proteins. *Arch. Biochem. Biophys. 519*, 91−102.
(57) Davydov, D. R., Davydova, N. Y., Sineva, E. V., and Halpert, J. R. (2015) Interactions among Cytochromes P450 in Microsomal Membranes: Oligomerization of Cytochromes P450 3A4, 3A5 and 2E1 and its Functional Consequences. *J. Biol. Chem. 290*, 3850−3864.
(58) Berka, K., Paloncyova, M., Anzenbacher, P., and Otyepka, M. (2013) Behavior of Human Cytochromes P450 on Lipid Membranes. *J. Phys. Chem. B 117*, 11556−11564.
(59) Vijayan, R., and Biggin, P. C. (2008) A steroid in a lipid bilayer: Localization, orientation, and energetics. *Biophys. J. 95*, L45−L47.
(60) Fernando, H., Rumfeldt, J. A., Davydova, N. Y., Halpert, J. R., and Davydov, D. R. (2011) Multiple substrate-binding sites are

DOI: 10.1021/acs.biochem.5b00079
Biochemistry 2015, 54, 2227−2239

retained in cytochrome P450 3A4 mutants with decreased cooperativity. *Xenobiotica 41*, 281−289.
(61) Ekroos, M., and Sjoegren, T. (2006) Structural basis for ligand promiscuity in cytochrome P 450 3A4. *Proc. Natl. Acad. Sci. U.S.A. 103*, 13682−13687.
(62) Sevrioukova, I. F., and Poulos, T. L. (2013) Dissecting cytochrome P450 3A4-ligand interactions using ritonavir analogues. *Biochemistry 52*, 4474−4481.
(63) Sevrioukova, I. F., and Poulos, T. L. (2014) Ritonavir analogues as a probe for deciphering the cytochrome P450 3A4 inhibitory mechanism. *Curr. Top. Med. Chem. 14*, 1348−1355.
(64) Yuki, H., Honma, T., Hata, M., and Hoshino, T. (2012) Prediction of sites of metabolism in a substrate molecule, instanced by carbamazepine oxidation by CYP3A4. *Bioorg. Med. Chem. 20*, 775−783.
(65) Jiang, Y., and Ortiz de Montellano, P. R. (2009) Cooperative effects on radical recombination in CYP3A4-catalyzed oxidation of the radical clock β-thujone. *ChemBioChem 10*, 650−653.
(66) Yang, J., Atkins, W. M., Isoherranen, N., Paine, M. F., and Thummel, K. E. (2012) Evidence of CYP3A allosterism in vivo: Analysis of interaction between fluconazole and midazolam. *Clin. Pharmacol. Ther. 91*, 442−449.
(67) Harrelson, J. P., Atkins, W. M., and Nelson, S. D. (2008) Multiple-ligand binding in CYP2A6: Probing mechanisms of cytochrome P450 cooperativity by assessing substrate dynamics. *Biochemistry 47*, 2978−2988.
(68) Harlow, G. R., and Halpert, J. R. (1997) Alanine-scanning mutagenesis of a putative substrate recognition site in human cytochrome P450 3A4. Role of residues 210 and 211 in flavonoid activation and substrate specificity. *J. Biol. Chem. 272*, 5396−5402.
(69) Tsalkova, T. N., Davydova, N. Y., Halpert, J. R., and Davydov, D. R. (2007) Mechanism of Interactions of α-Naphthoflavone with Cytochrome P450 3A4 Explored with an Engineered Enzyme Bearing a Fluorescent Probe. *Biochemistry 46*, 106−119.
(70) Cupp-Vickery, J., Anderson, R., and Hatziris, Z. (2000) Crystal structures of ligand complexes of P450eryF exhibiting homotropic cooperativity. *Proc. Natl. Acad. Sci. U.S.A. 97*, 3050−3055.
(71) Zhao, B., Guengerich, F. P., Bellamine, A., Lamb, D. C., Izumikawa, M., Lei, L., Podust, L. M., Sundaramoorthy, M., Kalaitzis, J. A., Reddy, L. M., Kelly, S. L., Moore, B. S., Stec, D., Voehler, M., Falck, J. R., Shimada, T., and Waterman, M. R. (2005) Binding of two flaviolin substrate molecules, oxidative coupling, and crystal structure of *Streptomyces coelicolor* A3(2) cytochrome P450 158A2. *J. Biol. Chem. 280*, 11599−11607.
(72) Jang, H. H., Davydov, D. R., Lee, G. Y., Yun, C. H., and Halpert, J. R. (2014) The role of cytochrome P450 2b6 and 2b4 substrate access channel residues predicted based on crystal structures of the amlodipine complexes. *Arch. Biochem. Biophys. 545*, 100−107.
(73) Shah, M. B., Wilderman, P. R., Pascual, J., Zhang, Q., Stout, C. D., and Halpert, J. R. (2012) Conformational adaptation of human cytochrome P450 2B6 and rabbit cytochrome P450 2B4 revealed upon binding multiple amlodipine molecules. *Biochemistry 51*, 7225−7238.
(74) Shoji, O., Kunimatsu, T., Kawakami, N., and Watanabe, Y. (2013) Highly selective hydroxylation of benzene to phenol by wild-type cytochrome P450BM3 assisted by decoy molecules. *Angew. Chem., Int. Ed. 52*, 6606−6610.
(75) Kawakami, N., Shoji, O., and Watanabe, Y. (2013) Direct hydroxylation of primary carbons in small alkanes by wild-type cytochrome P450BM3 containing perfluorocarboxylic acids as decoy molecules. *Chem. Sci. 4*, 2344−2348.
(76) Demaeght, P., Dermauw, W., Tsakireli, D., Khajehali, J., Nauen, R., Tirry, L., Vontas, J., Lummen, P., and Van Leeuwen, T. (2013) Molecular analysis of resistance to acaricidal spirocyclic tetronic acids in *Tetranychus urticae*: CYP392E10 metabolizes spirodiclofen, but not its corresponding enol. *Insect Biochem. Mol. Biol. 43*, 544−554.
(77) Mitchell, S. N., Stevenson, B. J., Muller, P., Wilding, C. S., Egyir-Yawson, A., Field, S. G., Hemingway, J., Paine, M. J., Ranson, H., and Donnelly, M. J. (2012) Identification and validation of a gene causing cross-resistance between insecticide classes in *Anopheles gambiae* from Ghana. *Proc. Natl. Acad. Sci. U.S.A. 109*, 6147−6152.
(78) Mast, N., Linger, M., and Pikuleva, I. A. (2013) Inhibition and stimulation of activity of purified recombinant CYP11A1 by therapeutic agents. *Mol. Cell. Endocrinol. 371*, 100−106.
(79) Mast, N., Li, Y., Linger, M., Clark, M., Wiseman, J., and Pikuleva, I. A. (2014) Pharmacologic Stimulation of Cytochrome P450 46A1 and Cerebral Cholesterol Turnover in Mice. *J. Biol. Chem. 289*, 3529−3538.
(80) Dixit, V., Hariparsad, N., Desai, P., and Unadkat, J. D. (2007) In vitro LC-MS cocktail assays to simultaneously determine human cytochrome P450 activities. *Biopharm. Drug Dispos. 28*, 257−262.
(81) Davydov, D. R. (2011) Microsomal monooxygenase as a multienzyme system: The role of P450-P450 interactions. *Expert Opin. Drug Metab. Toxicol. 7*, 543−558.
(82) Davydov, D. R., and Halpert, J. R. (2008) Allosteric P450 mechanisms: Multiple binding sites, multiple conformers or both? *Expert Opin. Drug Metab. Toxicol. 4*, 1523−1535.
(83) Denisov, I. G., Shih, A. Y., and Sligar, S. G. (2012) Structural differences between soluble and membrane bound cytochrome P450s. *J. Inorg. Biochem. 108*, 150−158.
(84) Johnson, E. F., and Stout, C. D. (2013) Structural diversity of eukaryotic membrane cytochrome P450s. *J. Biol. Chem. 288*, 17082−17090.
(85) Poulos, T. L., and Johnson, E. F. (2005) Structures of Cytochrome P450 Enzymes. In *Cytochrome P450: Structure, Function, Genetics* (Ortiz de Montellano, P. R., Ed.) 3rd ed., pp 87−114, Kluwer Academic/Plenum Publishers, New York.
(86) Mast, N., Liao, W. L., Pikuleva, I. A., and Turko, I. V. (2009) Combined use of mass spectrometry and heterologous expression for identification of membrane-interacting peptides in cytochrome P450 46A1 and NADPH-cytochrome P450 oxidoreductase. *Arch. Biochem. Biophys. 483*, 81−89.

DOI: 10.1021/acs.biochem.5b00079
Biochemistry 2015, 54, 2227−2239